LLNL-TR-811617

LAWRENCE
LIVERMORE
NATIONAL
LABORATORY

Determination of gamma-ray branching ratios for 95Zr and 147Nd

K. Kolos, N. D. Scielzo

June 14, 2020

This work performed under the auspices of the U.S. Department of Energy by Lawrence Livermore National Laboratory under Contract DE-AC52-07NA27344.

Determination of γ-ray branching ratios for ^{95}Zr and ^{147}Nd

K. Kolos and N. D. Scielzo

Lawrence Livermore National Laboratory

June 10, 2020

This work was performed under the auspices of the US Department of Energy (DOE) by the Lawrence Livermore National Laboratory (LLNL) under Contract No. DE-AC52-07NA27344, DE-AC02-06CH11357 (ANL), and DE-FG03-93ER40773 (TAMU), and the University of California under Contract No. DE-AC0376SF0098.

Summary

For many fission products, the γ rays emitted following β decay provide an easily-detectable signature that can be used to identify their quantities and distributions in a sample. As a result, γ-ray spectroscopy is often exploited to study fission-product yields (FPYs), provided sufficiently accurate information on the γ-ray branching ratio is available. However, in many cases, the uncertainties in the existing nuclear data are large enough that they compromise the precision achievable for modern experiments and applications. To address this need, we have developed a new experimental method that is well suited to precisely measure the γ-ray branching ratios in the β decay of long-lived fission products. The approach involves the production of a radiopure sample by implantation of a mass-separated ion beam from the CAlifornium Rare Isotope Breeder Upgrade (CARIBU) facility on a thin carbon foil. The emitted β-decay radiation is detected with a 4π gas proportional counter and a meticulously efficiency-calibrated high-purity germanium (HPGe) detector. As a first measurement to demonstrate the approach, we studied the γ-ray branching ratios of the strongest transitions following the β decay of ^{95}Zr and decay-daughter ^{95}Nb and determined these branching ratios to fractional precisions of 1%. We then applied this approach to determine the γ-ray branching ratios for the β decay of ^{147}Nd. The results for the γ-ray branching ratios are presented here and compared to previous results and evaluations.

Contents

Chapter 1

Introduction

1.1 Motivation

The fission product yields (FPYs) serve as key observables for understanding fission. Although gross features dealing with the double-peaked structure of the mass yield curve are interpreted within the context of fission theory [1], the yields of individual products and their dependence on the excitation energy of the fissioning system remain poorly understood. The LLNL-LANL-TUNL Collaboration has a history of successfully measuring the long-lived (cumulative) FPYs in neutron-induced fission [2, 3, 4, 5, 6, 7, 8]. These experiments rely on determining the FPYs through the detection of the characteristic γ rays emitted following their β decays.

For instance, the detection of the most intense γ rays in the decay of the long-lived fission products ^{95}Zr and ^{147}Nd are used to determine the production of the A=95 and A=147 chain yields in a sample [2, 9]. The interpretation of measurements that rely on γ-ray spectroscopy therefore depends on a precise knowledge of the absolute intensities of the γ-rays emitted following the β decay of the isotopes studied. The uncertainty in the absolute intensity directly leads to an uncertainty at the same level in the deduced FPY.

The decay of ^{95}Zr is an example where the nuclear data for β-decay transition strengths and the corresponding γ-ray branching ratios are well understood. In this case, the γ-ray branching ratios have previously been measured to a relative precision of about 0.5% [10] [11] and there is good agreement between multiple measurements.

However, for many other isotopes, the nuclear data is on much shakier ground. The decay of ^{147}Nd is an example where the situation is not simple. In the latest Nuclear Data Sheet (NDS) evaluation [12] published in 2009, the branching ratio for the 531.0-keV γ ray (the transition typically used to identify the presence of ^{147}Nd in a sample) is listed as 13.4(11)%. For the same transition, the Decay Data Evaluation Project (DDEP) recommends a branching ratio of 12.7(9)%. The NDS and DDEP evaluations differ by about 5% for this γ-ray branching ratio and the overall relative uncertainty is 7-8%, which is quite large. To make matters worse, the value listed online on the National Nuclear Data Center (NNDC) website [13] for this transition has changed over the last few years, and now lists a greatly reduced uncertainty of 2.2%, despite the last relevant measurement having been published in 1997 [14].

Several challenges arise in efforts to precisely determine the intensities of γ rays emitted following the β decay of long-lived fission products such as ^{95}Zr and ^{147}Nd. Radionuclides with half-lives longer than $\sim$1 day typically have Q_β values that are less than 1 MeV and emit low-energy β particles that are easily attenuated in the material used to suspend the sample or in dead layers of the detection system. Even for the β particles that reach the active region of the detector, the threshold of the detection system can have a significant impact on the detection efficiency. In addition, the radiopurity of the sample must be carefully controlled because β particles emitted from contaminants are difficult to distinguish from those emitted from the nuclei of interest. The measurements also rely on detailed characterizations of the detection system, especially the γ-ray detector, for which an absolute efficiency calibration is typically needed.

In this report, we utilize a new experimental approach that addresses the challenges that arise in efforts to measure the intensities of γ rays emitted following the β decay of fission products to a precision of 1% or better. We performed a measurement of the γ-ray branching ratios in the decay of ^{95}Zr to verify the reliability of the approach, and then applied the methodology to precisely determine the γ-ray intensities in the decay of ^{147}Nd.

1.2 Overview of measurement approach

The method we developed takes advantage of advances in the production and mass separation of low-energy radioactive beams of fission products developed at the CAlifornium Rare Isotope Breeder Upgrade (CARIBU) facility [15, 16] at Argonne National Laboratory (ANL). The fission products are implanted in thin carbon foils from which the emitted radiation emerges with minimal attenuation. These samples are then shipped to Texas A&M University (TAMU) in College Station, Texas, and inserted into a 4π gas proportional counter to detect β particles. The γ rays are detected with a meticulously efficiency-calibrated HPGe detector [17, 18, 19]. We determine the γ-ray intensities (I_γ) for a particular transition from the β-γ coincidence detection rate ($R_{\beta\gamma}$) relative to the β-particle detection rate from the decay of the isotope of interest (R_β), through the relation

$$I_\gamma = \frac{R_{\beta\gamma}}{R_\beta}\frac{1}{\varepsilon_\gamma}\frac{\varepsilon_\beta}{\varepsilon_{\beta'}}. \tag{1.1}$$

Here ε_γ is the photopeak efficiency of the HPGe detector for detecting the γ ray of interest, $\varepsilon_{\beta'}$ is the efficiency for detecting the β particles emitted in coincidence with that γ ray, and ε_β is the efficiency for detecting all β decays of the isotope of interest in the 4π gas counter. The ratio $\varepsilon_\beta/\varepsilon_{\beta'}$ differs slightly from unity because the β-particle spectra under consideration have different end-point energies and hence different fractional threshold losses.

As a first measurement with this approach, we studied the β decay of the fission-product ^{95}Zr and the accompanying daughter-nucleus ^{95}Nb. These nuclei have simple decay schemes, with large γ-ray intensities that have previously been established with relative precisions of better than 0.5% [10] [11]. In addition, the 64-day half-life of ^{95}Zr provides ample time to collect the sample at ANL and transport it to the measurement location at TAMU.

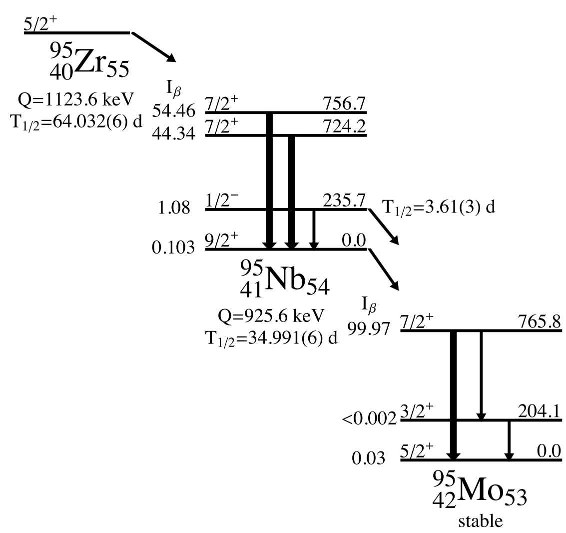

Figure 1.1: Decay schemes of ^{95}Zr and ^{95}Nb showing only the relevant decay properties. For simplicity, the β branching ratios (I_β) in the decay of ^{95}Nb to ^{95}Mo presented here, represent only the decays from the ground state of ^{95}Nb. All excitation energies are in keV. The data are taken from Ref. [10].

The relevant decay properties of ^{95}Zr and ^{95}Nb are shown in Fig. 1.1. The ^{95}Zr nucleus decays primarily by allowed transitions to the excited states at 756.725(12) keV (with β-particle end-point energy $E_{\beta_{max}}$ = 366.9(18) keV and with a β transition strength I_β=54.46(22)%) and 724.192(4) keV ($E_{\beta_{max}}$= 399.4(18) keV, I_β=44.34(22)%) which deexcite directly to the ground state of ^{95}Nb. The ^{95m}Nb isomeric state at 235.69(2) keV and the ground state of ^{95}Nb are directly populated by first- and second-forbidden transitions, respectively, with branching ratios previously determined to be 1.08(7)% and 0.103(11)%. The ^{95}Nb ground state decays by an allowed transition almost entirely to the 765.803(6) keV excited state in ^{95}Mo which deexcites by γ-ray emission directly to the ground state. The ^{95m}Nb isomeric state has a half-life of 3.61(3) days and decays predominantly by internal transition to the ground state of ^{95}Nb (97.5(1)%) in the evaluation in Ref. [11] or 94.4(6)% in the evaluation in Ref. [10]), with the remaining contribution from β decay to states in ^{95}Mo. The internal transition is highly converted, with a total conversion coefficient α=2.78(4) [20].

We used the high-intensity γ-ray transitions in the decay of ^{95}Zr and ^{95}Nb to determine, *in situ*, the efficiency of the 4π gas counter for detecting β particles. This information allowed us to scrutinize the β-detector performance and establish the detection threshold. The efficiencies of the dominant transitions in the decays of ^{95}Zr and ^{95}Nb can be obtained with a comparison of γ-ray detection rates with and without the detection of the coincident β particle. The simulations of the experimental apparatus were carried out to properly account for the correlations in the detection efficiencies for these transitions, and to allow the efficiency of β-decay branches without a prompt γ ray to be deduced. These simulations are required to characterize the detection efficiency for the more complicated decay schemes encountered for most other fission products.

We applied this measurement approach to determine the γ-ray intensities following the decay of ^{147}Nd. ^{147}Nd β decays with a 10.98(1)-day half-life [12] and a relatively small Q value of 896.0(9) keV to multiple states in ^{147}Pm, with most of the β-decay intensity populating the excited states at 91.1 keV and 531.0 keV. The decay properties are shown in Fig. 1.2. The ^{147}Pm daughter nucleus β decays with a half-life of 2.6234(2) yr and a Q value of 224.6(4) keV to the ground state of stable ^{147}Sm in over 99.99% of the decays. As mentioned earlier, the current evaluations of the decay properties of ^{147}Nd show some discrepancies. The latest NNDC evaluation available online [12] recommends values of 28.1(7)% and 13.4(3)% for the intensities of the 91.1-keV and 531.0-keV γ rays, respectively, based solely on the results in Ref. [14], with relative uncertainties of about 2% coming directly from that measurement. The DDEP evaluation for ^{147}Nd [21] recommends absolute γ-ray branching ratios of 28.4(18)% and 12.7(9)%, respectively, with relative uncertainties of about 7% based on the results in Refs. [22, 14].

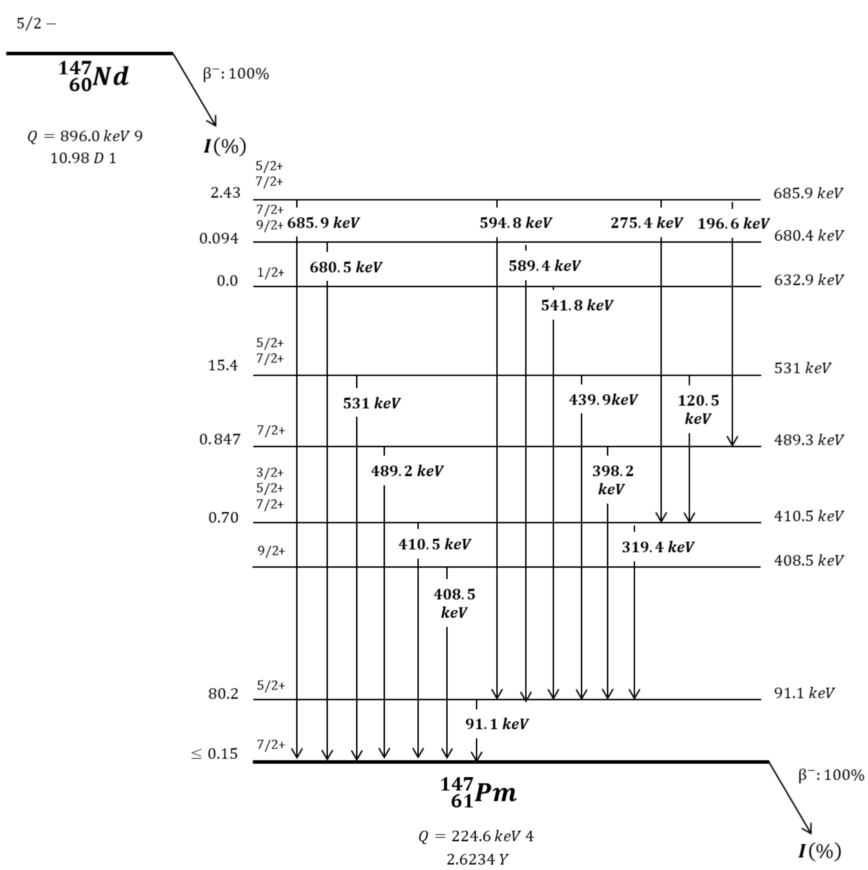

Figure 1.2: Decay scheme of ^{147}Nd showing the relevant decay properties. The decay properties shown are from the NNDC evaluation [12].

Chapter 2

Proof-of-principle demonstration - ^{95}Zr

2.1 Source production

A ^{95}Zr sample free of any radioisotope contamination (except for the decay daughter) was produced at the CARIBU facility [15, 16] by collection of fission products with A=95 from the spontaneous fission of a ∼1 Ci ^{252}Cf source. The isotopes in this mass chain with the highest yields are the short-lived ^{95}Sr ($T_{1/2}$ = 23.9 s) and ^{95}Y ($T_{1/2}$ = 10.3 min) which subsequently decay to produce a sample of the long-lived ^{95}Zr isotope.

The fission products were thermalized using a large helium-filled gas catcher and extracted as a continuous low-energy ion beam from the nozzle of this device using a combination of gas flow and electric fields [15, 16]. The emerging ions were accelerated with a potential of 36 kV and sent through an isobar separator [23]. The mass slits of the isobar separator were set to select only ions with mass-number-to-charge ratio A/Q=47.5, corresponding to A=95 fission products in the 2^+ charge state. This beam of primarily ^{95}Sr and ^{95}Y ions was then delivered to a collection point, where the isotopes were implanted into a carbon foil. The decay of the accumulated isotopes built up a population of the long-lived ^{95}Zr fission product.

The carbon foil was 41 μg/cm^2 (200 nm) thick and suspended over an 11-mm-diameter opening on an aluminum holder. The foil and holder were located behind a 7-mm-diameter aperture to ensure that the ions would only be implanted in the exposed area of the carbon foil. The foil thickness was selected to minimize the attenuation of the emitted β particles while being mechanically rugged enough for handling and shipping. The fission products were implanted at a depth of ∼50 nm, or about 25% of the thickness of the carbon foil. Prior to the sample accumulation, we optimized the delivery of the beam by temporarily moving 1-mm-thick silicon detectors in place of the carbon foil. As ions accumulated ions on an aluminum foil in front of the detector, the count rate of the detected β particles emitted from the short-lived species was maximized. Two detectors were used: first one located behind a 25-mm-diameter aperture, and then one behind a 7-mm-diameter aperture to match the size of the aperture in front of the carbon foil.

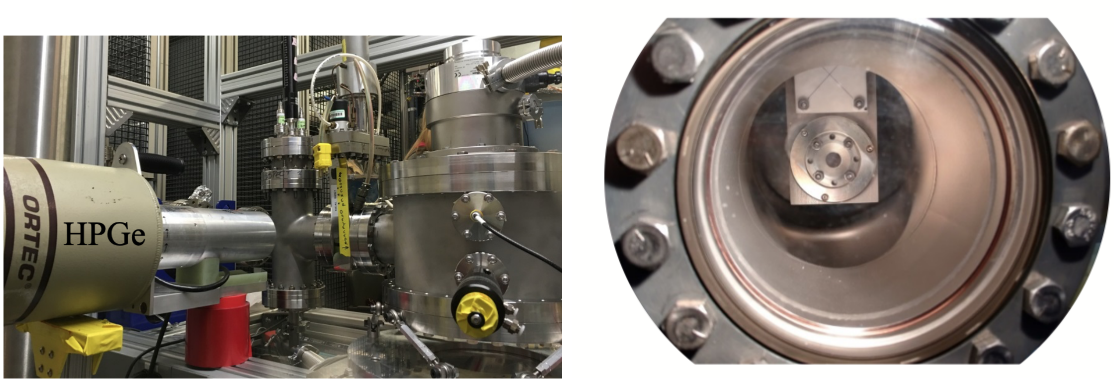

Figure 2.1: (left) Placement of the cross on the beam line with a HPGe detector viewing the collection point. (right) Looking directly down the beam line through a vacuum window on the backside of the cross, one can see the foil positioned in the path of the oncoming beam.

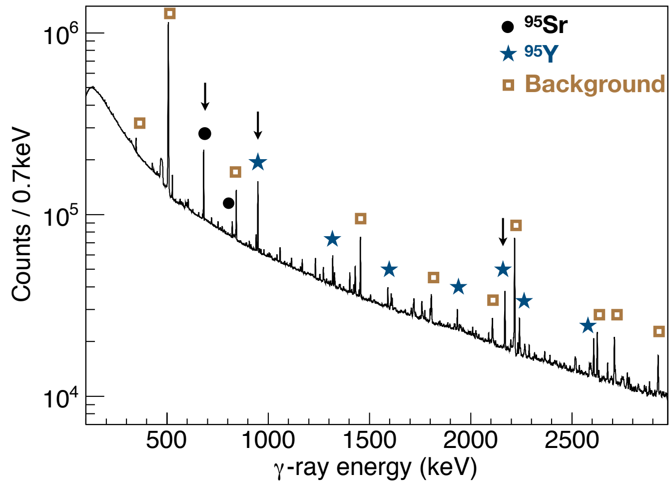

Figure 2.2: The total γ-ray spectrum observed during the collection of A=95 fission-product ions at the CARIBU facility. The 685.6-keV γ rays from the decay of ^{95}Sr and the 954.0-keV and 2175.6-keV γ rays from the decay of ^{95}Y were used to determine the beam intensity during the sample collection. The peaks from these γ rays are identified by arrows.

The integrated beam intensity delivered to the foil was determined every few hours by counting the total number of 685.6-keV γ rays from the decay of ^{95}Sr and the 954.0-keV and 2175.6-keV γ rays from the decay of ^{95}Y detected with a HPGe detector continually monitoring the isotope collection location. The summed γ-ray spectrum from all the individual measurements obtained over the course of the sample collection is shown in Fig. 2.2. The prominent peaks in this spectrum can all be attributed to the decays of ^{95}Sr and ^{95}Y or to room background. The room background was measured before implantation and was used to characterize any interference present at energies near the peaks of interest.

The β-delayed neutron emission of any collected ^{95}Rb (with a neutron-emission probability of $P_n = 8.7\%$) and ^{95}Kr ($P_n = 2.87\%$) ions could produce a small amount of A=94 activity, but this has no effect on the measurement because the longest-lived radioisotope in this mass chain is ^{94}Y with a half-life of 18.7 min and therefore would have decayed away several hours after implantation.

We used the time-history of the ^{95}Sr and ^{95}Y collection to gauge the number of ^{95}Zr atoms accumulated in the foil and to precisely calculate the evolution of the ^{95}Zr/^{95}Nb ratio in the sample throughout the course of the collection and subsequent decay counting. Over a collection time period spanning 6.4 days (including a total of 0.7 days without beam), we implanted in the graphite foil $A = 95$ ions at just over 2100 ions/s, resulting in a ^{95}Zr activity of about 140 Bq. This sample was shipped to TAMU and arrived there within two days of the end of the collection.

2.2 β-particle counting

At TAMU, the sample was inserted into the center of the 4π gas proportional counter for β-particle detection. The design of this counter was based on the detector described in Refs. [24, 25] and consisted of two separate gas cells machined from copper, each equipped with a 12.7-μm-diameter gold-plated tungsten anode wire. Modifications were made to eliminate the internal windows present in the previous design which separated the sample from the active gas volume [26]. The aluminum holder supporting the carbon foil with activity was inserted between the two detector halves. Once in place, the two halves were bolted together and a seal was formed by compressing o-rings housed within grooves in the copper chamber against the aluminum holder frame. On the two exterior faces of the detector, 12.7-μm-thick Havar windows sealed each gas cell. Methane gas at atmospheric pressure was continuously flushed through both cells. Therefore, the carbon foil was directly in contact with the methane gas and any particles emerging from the foil would immediately enter the active volume of the gas counter.

The handling of the signals from the 4π gas counter was analogous to that described in Ref. [27]. The anode pulses were passed to a preamplifier and a timing-filter amplifier, then sent to a constant fraction discriminator and then gate generator.

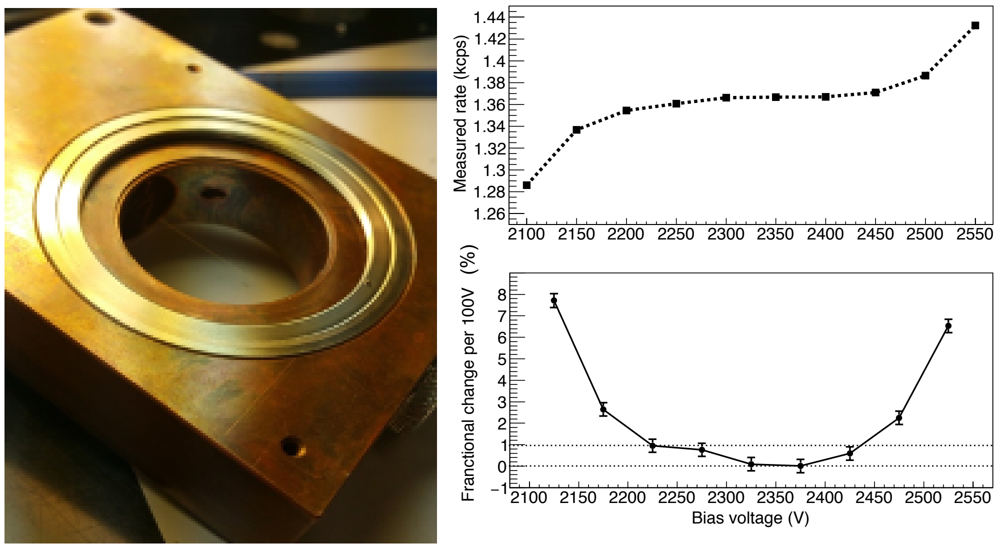

Figure 2.3: (left) Picture of the 4π gas counter opened up. (right) (top) The gas counter count rate in the region of the voltage plateau measured with a ^{147}Nd source placed in the center of the device. (bottom) The fractional change in the count rate per 100 V applied to the detector. Between 2.25 and 2.45 kV, the change was less than 1% per 100 V. The detector was operated at 2.40 kV for the ^{95}Zr measurements.

We optimized the detector operating parameters through traditional plateau measurements by detecting the count rate as a function of the voltage applied to the anode wires. For these measurements, sources were either inserted into the center of the detector, or placed outside of the Havar window. For the plateau measurements performed just prior to the ^{95}Zr decay counting, we used a 1.4-kBq ^{147}Nd sample, made in an analogous way to the ^{95}Zr sample at CARIBU. That sample had 10 times higher activity than the ^{95}Zr sample, which allowed for the voltage optimization to be carried out in a reasonable amount of time. The result presented in Fig. 2.3 shows an operating region between 2.25 kV and 2.45 kV where the count rate increases by less than 1% for each additional 100 V applied to the detector. Based on this measurement, we chose to operated the gas counter at 2.40 kV. Additional plateau measurements with a ^{90}Sr sealed source placed outside the counter were performed after the completion of the ^{95}Zr measurements; these plateau results confirm there had been no change in detector performance over the course of the measurement.

2.3 γ-ray detection

The γ rays emitted from the sample were detected with a meticulously efficiency-calibrated 70%-relative-efficiency ORTEC HPGe coaxial detector [17, 18, 19]. A cylindrical lead-plastic-copper layered shield was placed around the HPGe detector to attenuate the room background by about a factor of three over a wide range of energies and improve the signal-to-background ratio in the γ-ray spectrum. The detection setup used in this experiment is shown in Fig. 2.4.

The original HPGe detector absolute efficiency calibration was done at a fixed source-to-detector distance of 151.0 mm. The efficiencies were determined over the energy range of 50-1500 keV with the CYLTRAN [28] simulation to 0.2% precision [18, 19]. However, for the current measurements, the source-detector distance was inadvertently set to 152.87(10) mm, as confirmed by measurements with a laser system [29] made subsequent to the experiment. The corresponding HPGe detector efficiencies (ε_γ) at that distance obtained from the CYLTRAN simulation are about 2.2% smaller than what would have applied at the nominal distance, and were assigned slightly higher relative uncertainties to account for the added uncertainty surrounding the distance error (0.3% as compared to 0.2%). They are reported in Table. 2.1.

2.4 Data collection

For these measurements, the γ-ray singles were recorded with ORTEC EASY MCA handled by MAESTRO and the $\beta - \gamma$ coincidences were recorded event-by-event with a program

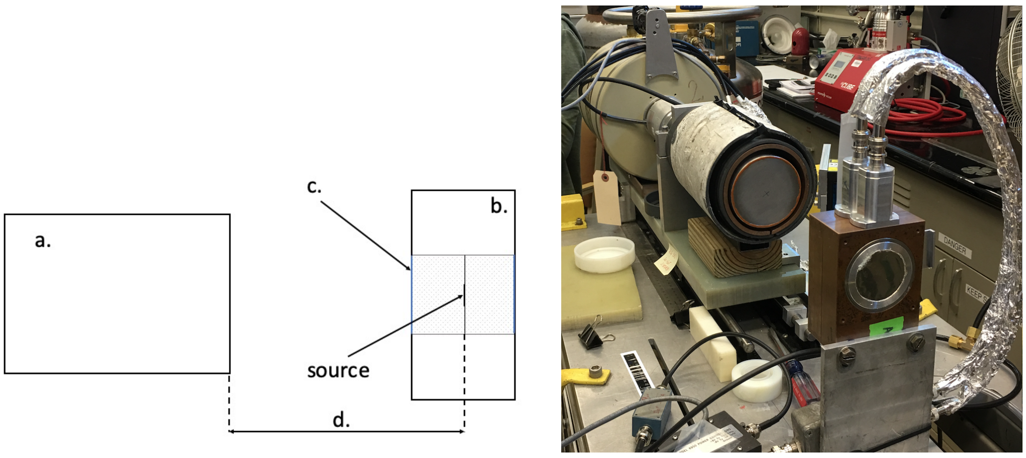

Figure 2.4: The detector setup used during the experiment consisting of (a.) the HPGe detector and (b.) the 4π gas counter with external Havar windows (c.). The aluminum holder supporting the carbon foil with the implanted ^{95}Zr (source) was inserted into the center of the 4π gas counter. The HPGe detector to source distance (d.) was 152.87(10) mm.

Table 2.1: HPGe detector efficiencies for the γ rays emitted following ^{95}Zr and ^{95}Nb decay.

Isotope	E_γ	ϵ_γ (%)
^{95}Zr	724.2 keV	0.2977(9)
^{95}Zr	756.7 keV	0.2884(9)
^{95}Nb	765.8 keV	0.2860(9)

written in the KmaxNT environment [30] previously used in precise branching-ratio measurements (see e.g. [27, 31, 32]). For β and γ-ray signals arriving within 2 μs of each other, considered as "coincident", a master-gate was generated and four parameters were measured: the β energy deposition in the 4π gas counter, the γ-ray energy deposition in the HPGe detector, the time difference between the detection of the two particles, and the absolute time of the coincidence. The number of HPGe and 4π-gas-counter triggers were also stored.

Coincidence data were collected in cycles for 54.93 s out of every 60 s [33, 32] over a time span of 7.5 days with the KmaxNT system, and a total measurement time of 5.93×10^5 s (10799 cycles). The settings for the coincident data collection were based on thoroughly-vetted settings used in multiple previous measurements by the TAMU group. In these previous measurements, 5.07 s out of every 60 s were used to accommodate the transport of activity on a moving tape collector – in our experiments, this time just served as dead time for the measurement as the sample location was fixed. The total measurement time for γ-ray singles, recorded with MAESTRO in parallel with the coincidence system, was nearly 8 days (live time of 6.79×10^5 s). The γ-ray singles background was measured for 9.7 days (8.42×10^5 s) before decay counting. The 4π-gas-counter background rate measured with a blank aluminum holder, and without the carbon foil, was 0.69(1) counts per second (cps). The background coincident count rate between the 4π gas counter and the HPGe detector was negligible.

2.5 Coincidence rates ($R_{\beta\gamma}$)

The time difference between the β-particle and γ-ray signals for coincident events is presented in Fig. 2.5. The peak centered near 1 μs corresponds to the true coincidence events and the flat distribution which extends to either side arises from random coincidences. We produced a γ-ray spectrum free of random-coincidence events by first gating on the prompt time-difference peak and then subtracting normalized random coincidences obtained by gating on the flat regions on either side of the prompt peak. The resulting $\beta - \gamma$ coincidence spectrum Fig. 2.6 (a) contains only the three peaks at 724.2 and 756.7 keV from the decay of ^{95}Zr and 765.8 keV from the decay of ^{95}Nb. No coincident peak at 235.6 keV was observed from the decay of ^{95m}Nb because the 3.61-day lifetime of the state significantly delays the emission of the γ ray.

To obtain the peak areas, we used the fitting procedure described in Ref. [18], which is the same one used for the efficiency calibration of the HPGe detector. It employs a modified

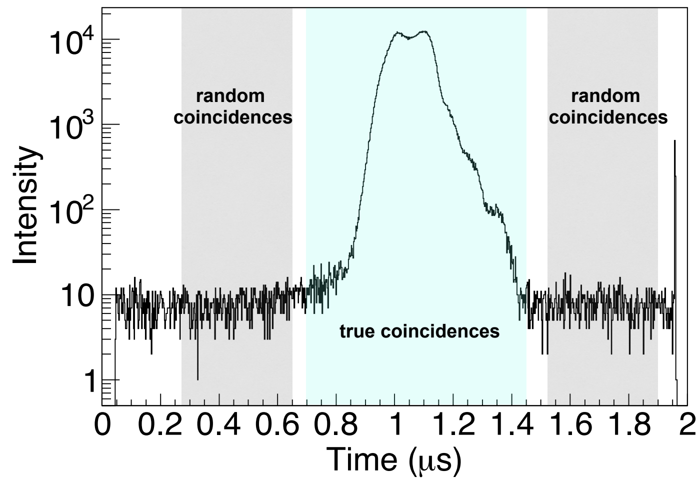

Figure 2.5: Measured time-difference spectrum for coincidences between the 4π gas counter and the HPGe detector.

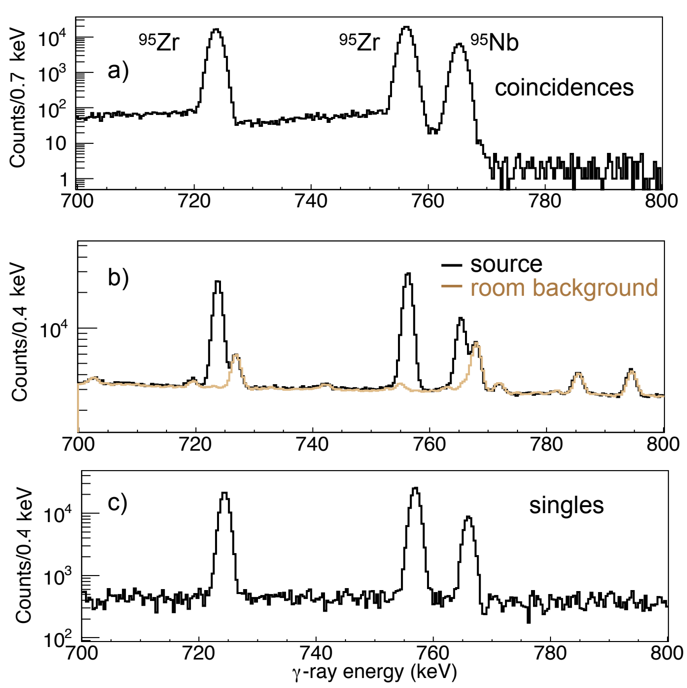

Figure 2.6: (a) The γ-ray spectrum measured in coincidence with β particles. The peaks of interest are labeled by their β-decay parent. (b) The γ-ray singles spectrum and the room-background spectrum, the latter is scaled by the measurement live times. (c) The γ-ray singles spectrum from the source obtained by subtracting the room background, with 300 counts added to each bin for plotting purposes. The resolution obtained for with the KmaxNT system for the coincidence spectrum was slightly worse than the data obtained with the MAESTRO system.

version of GF3, the least-squares peak-fitting program in the RADWARE series [34]. This method determines the number of counts in the peaks by integrating the spectrum above a well-defined background. The number of counts in the three peaks of interest, at 724.2, 756.7 and 765.8 keV, were $9.63(4) \times 10^4$, $1.163(5) \times 10^5$ and $3.81(3) \times 10^4$, respectively.

We calculated the rates by dividing these areas by the live time of the measurement. The measurement dead time due to the count rates changed the inferred rates by less than 0.1%. The resulting detection rates for the 724.2-keV, 756.7-keV, and 765.8-keV γ-ray peaks were 0.1626(8), 0.1962(8) and 0.0642(5) cps, respectively.

2.6 4π gas counter efficiency

2.6.1 GEANT4 simulated efficiencies

The β-particle energy spectra for the decays of ^{95}Zr and ^{95}Nb were generated with a Monte Carlo decay code originally developed in Ref. [35] and adapted for this work. The one notable modification that had to be implemented in the code was the use of an analytical non-relativistic approximation [36] to the Fermi function to better determine the values below 20 keV. Previously, the Fermi functions were generated from a cubic spline of the tabulated values in Ref. [37]; however, this approach did not give accurate results below about 5 keV, an energy region crucial to this work. The resulting spectra for ^{95}Zr and ^{95}Nb are shown in Fig. 2.7. As can be seen, the energy distributions for both nuclei are heavily weighted towards low-energy β particles with the peaks of the distribution being at nearly zero energy.

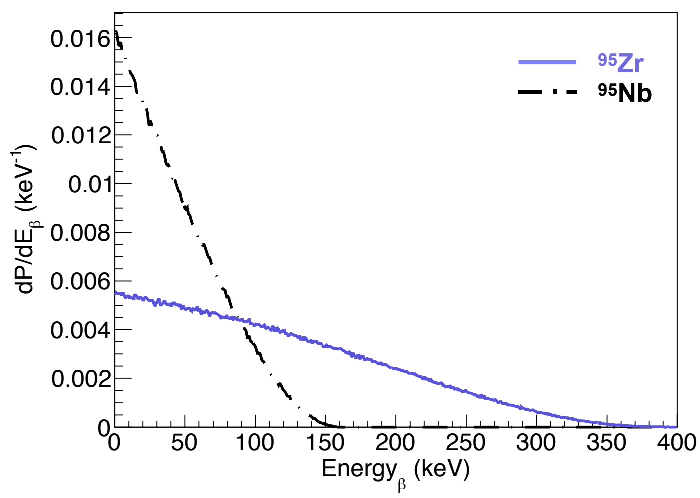

Figure 2.7: Theoretical probability distribution function of the β energy spectra emitted in the decays of ^{95}Zr and ^{95}Nb. Both distributions are heavily weighted towards low-energy β particles due to the low energy of the transitions and the relatively large Z of the nuclei.

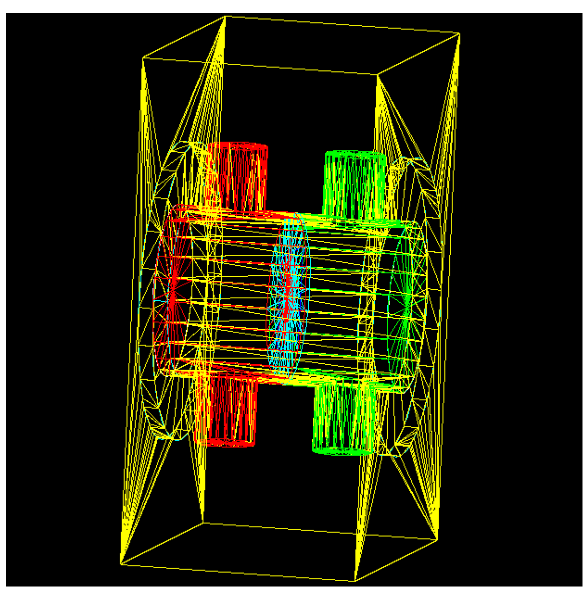

Figure 2.8: Schematic view of the 4π gas counter geometry in the GEANT4 simulation. The interior gas volumes of the two halves of the counter are shown in red and green. The aluminum holder and foil containing the activity is indicated in blue.

The particles emitted in the decay were propagated through the detector using the Monte Carlo based toolkit, GEANT4 (GEometry ANd Tracking) [39], which incorporated the G4EmLivermorePhysics package to account for interactions down to 10 eV. In addition, we updated the stopping power libraries for graphite to the recommended by the IRCU90 report [40] that were not included in the standard GEANT4 release.

The detector geometry, shown in Figure 2.8, consisted of two gas cells made of copper with exterior Havar windows, the methane gas, the carbon foil, and the aluminum holder. The depth of the ion deposition in the carbon foil was calculated with TRIM [38] software assuming 72-keV beams of ^{95}Sr and ^{95}Y ions (Fig. 2.9). The energy deposition inside the counter and the position of the interaction were recorded for each event.

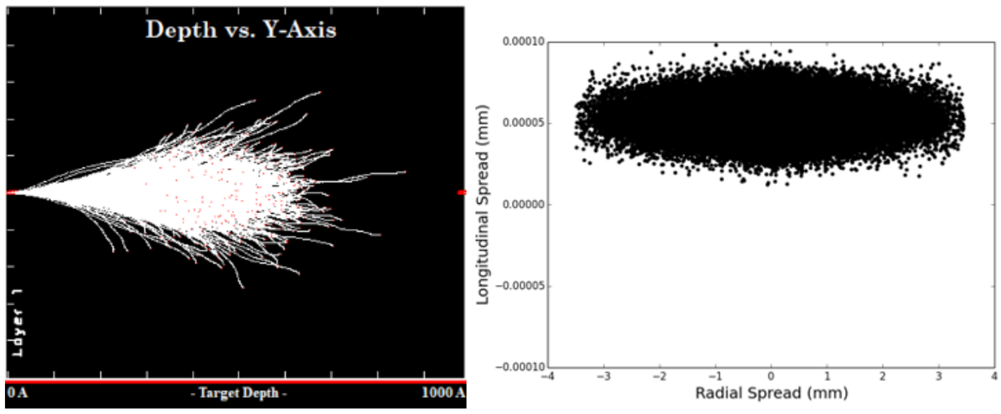

Figure 2.9: Depth of the ion deposition in the carbon foil calculated for a 72-keV beam of A=95 ions calculated with TRIM [38].

2.6.2 Experimentally determined efficiencies

The $\varepsilon_\beta/\varepsilon_{\beta'}$ efficiency ratio of the 4π gas proportional counter in Eq. 1.1 deviates from unity because the β-particle energy spectra in the ratio are not identical, and a different fraction of low-energy particles is lost to absorption in the carbon foil or to the electronic threshold of the counter. We determined the efficiency ratio using simulations of the detector response to the β-decay spectra under consideration.

We obtained the absolute efficiencies for the three transitions from the data using the ratio of the $\beta-\gamma$ coincident rate to the rate, R_γ, of that particular γ ray detected in singles:

$$\varepsilon_{\beta'} = \frac{R_{\beta\gamma}}{R_\gamma}. \tag{2.1}$$

The measured coincidence detection rates, $R_{\beta\gamma}$, for the 724.2-keV, 756.7-keV, and 765.8-keV γ-ray peaks were 0.1626(8), 0.1962(8) and 0.0642(5) cps, respectively, as discussed in Section 2.5.

The singles rates R_γ were obtained from the measured γ-ray singles spectrum with the room background subtracted (see Fig. 2.6 (c)). To determine the γ-ray peak areas we employed the same fitting procedure as for the coincidence spectra. The resulting rates R_γ for the three transitions at 724.2, 756.7, and 765.8 keV were 0.1692(8), 0.2045(8) and 0.0687(8) cps, respectively. The coincidence and singles data were collected with two different data acquisition systems and at a slightly different times with the singles measurements starting about 12 hours earlier than the coincidence. Therefore, to directly compare the rates, we had to apply a correction to the average activity expected at the time of the singles measurement. The corrected singles rates R_γ for the three transitions at 724.2, 756.7, and 765.8 keV were 0.1669(8), 0.2029(8), and 0.0696(8) cps for the three transitions.

Based on these results, the 4π gas counter efficiencies for detecting the β particles emitted in coincidence with the 724.2-keV and 756.7-keV γ rays in the decay of ^{95}Zr were determined to be 97.4(4)% and 96.7(3)%, respectively. The efficiency for detecting the β particles emitted in coincidence with the 765.8-keV γ ray in the decay of ^{95}Nb was 92.2(11)%. Note that in the ratio, the statistical uncertainties associated with the total number of counts are highly correlated (and therefore reduce substantially), although the contribution from background subtractions were considered uncorrelated and therefore added in quadrature. The two ^{95}Zr decay transitions have similar maximum β-particle energies, $E_{\beta_{max}}$, of 366.9(18) keV and 399.4(18) keV, so they are expected to have nearly identical efficiencies. For ^{95}Nb, $E_{\beta_{max}}$ is only 159.8(5) keV and the efficiency is correspondingly lower.

2.6.3 Detection threshold determination

To determine the detection threshold, we compare the energy depositions in the detector with the Monte Carlo simulations, as shown in Fig. 2.10. The energy calibration of the pulse-height spectrum was adjusted so that the peaks of the distributions agree with the Monte Carlo spectrum. Although differences in the spectra can be seen at energies >20 keV, potentially due to effects such as imperfect charge collection in the detector or a nonlinear response of the electronics, it is the low-energy portion of the spectrum that influences the

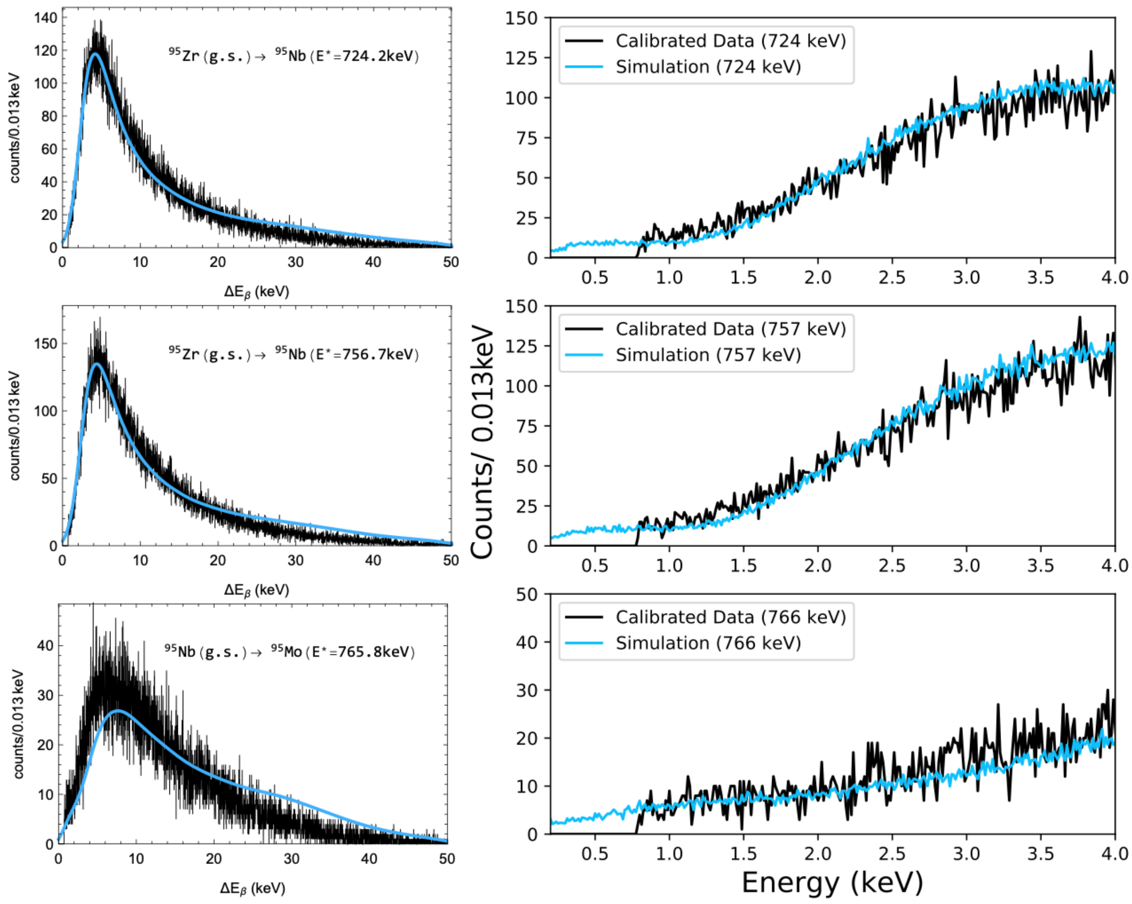

Figure 2.10: Energy deposition in the 4π gas counter detector from the β particles detected in coincidence with the 724-keV γ rays and 757-keV γ rays from the decay of ^{95}Zr, and the 766-keV γ rays from the decay of ^{95}Nb. The measured spectra (black) are compared to the simulation results (blue). Although differences in the spectra can be seen, potentially due to effects such as imperfect charge collection in the detector or a nonlinear response of the electronics, it is the low-energy portion of the spectrum (expanded on the right) that influences the detection efficiency.

detection efficiency. Based on the energy spectrum, the electronic threshold appears to be 0.7(1) keV.

As a secondary verification method to find the best match for the β particle detection energy threshold, we compared the measured and simulated 4π gas counter efficiencies as a function of the threshold. With the χ^2 minimization method, we found the best agreement at the threshold of 1.1(4) keV (see Fig.2.11). This result is consistent with the value of 0.7(1) keV determined from the energy spectra that was chosen as the threshold in further analysis.

With this information, we can use the simulation to calculate the efficiencies for detecting all β-decay and conversion-electron decay modes. The results of the 4π gas counter efficiencies at the 0.7(1) keV threshold for the three transitions compared with the measured values, as well as the simulated efficiency ratios $\varepsilon_\beta/\varepsilon_{\beta'}$ used in the γ-ray intensity determinations, are presented in Table 2.2. The efficiency for detecting the conversion electrons emitted in these decays is essentially 100%.

2.7 Determination of R_β

A total of 8.8593 $\times 10^7$ counts was recorded in the 4π gas counter over the course of the $\beta - \gamma$ coincidence measurement, which resulted in an average detected rate of 148.66(2) cps above the background rate. To obtain the value of R_β for ^{95}Zr, ^{95}Nb, and ^{95m}Nb present in the sample, we determined the fraction each one contributed to the total detected count rate over the course of the measurement from the time dependence of the implantation at CARIBU and the Bateman solutions (Fig. 2.12). Over the time of the coincidence measurement, the fraction of the total activity from the decays of ^{95}Zr, ^{95}Nb, and ^{95m}Nb were determined to be 0.8345(9), 0.1572(9), and 0.0083(5), respectively.

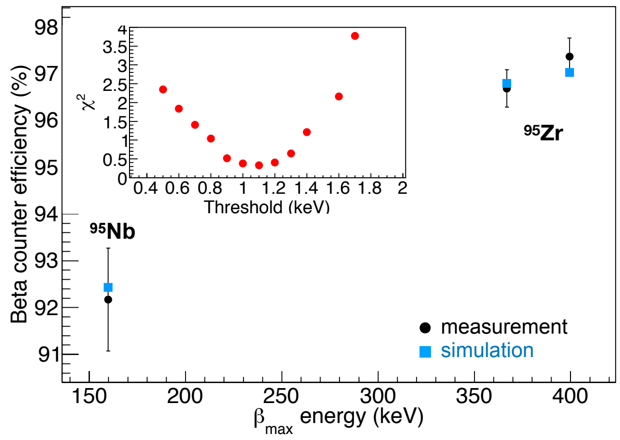

Figure 2.11: Comparison of the measured gas counter efficiencies for the three transitions to simulation results with a 1.1 keV threshold. The insert shows the χ^2 values obtained from the difference between the measured and simulated efficiency values spanning a range of thresholds. The minimum of the χ^2 results indicated the detector threshold was 1.1(4) keV.

Table 2.2: The 4π gas counter detection efficiencies for β-particle detection in the decay of ^{95}Zr and ^{95}Nb. The table shows the comparison of measured efficiencies and simulation results with a threshold of 0.7 keV for the three transitions with γ rays of energies 724.2, 756.7 and 765.8 keV, the efficiency ratio ($\varepsilon_\beta/\varepsilon_{\beta'}$) for the 4π gas counter obtained from the GEANT4 simulation and used in the γ-ray intensity calculations, and the efficiency for each isotope ε_β used in R_β calculation.

$E_{\beta_{max}}$	$\varepsilon_{\beta'}$ (%) (meas.)	$\varepsilon_{\beta'}$ (%) (GEANT4)	$\varepsilon_\beta/\varepsilon_{\beta'}$
399.4(18)	97.4(4)	97.40	0.9988(1)
366.9(18)	96.7(3)	97.16	1.0013(1)
159.8(5)	92.2(11)	92.81	1.0000(1)

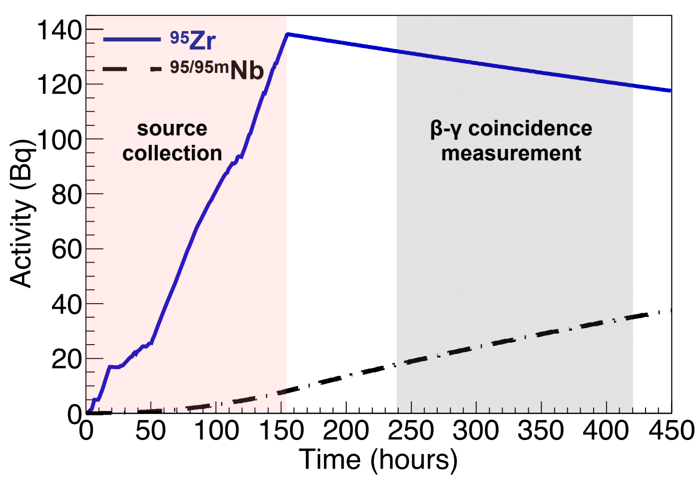

Figure 2.12: Build up and decay of ^{95}Zr and the daughter ^{95}Nb over the duration of the experiment. The shaded areas indicate the time of the source production at CARIBU and the time of the coincidence measurement at TAMU. The shape of the build up of the ^{95}Zr activity during the source production was the result of variations in the CARIBU beam intensity.

With the activity ratios in hand, we determined the relative contribution to the count rate of the 4π gas counter from each species after accounting for the different β-particle detection efficiencies. The required efficiency of the 4π gas counter for each isotope, ε_β, used in this calculation is described in Section 2.6. Note that the conversion electrons emitted from the internal transition decay of ^{95m}Nb contribute to the total number of detected β singles. The resulting fraction of the total detector count rate from ^{95}Zr, ^{95}Nb, and ^{95m}Nb was 0.8423(9), 0.1514(9) and 0.0063(5), yielding absolute detector count rates of 125.22(14) cps, 22.50(13) cps and 0.93(7) cps, respectively.

2.8 Branching ratios

We determined the γ-ray branching ratios, I_γ, for the γ-rays transitions in the decay of ^{95}Zr, with precision of 0.5%, and with 1% precision for the γ-rays transition in the decay of ^{95}Nb. These results and the contributions to the uncertainties are presented in Table 2.3. The dominant component for all three peaks of interest comes from the statistics in the $\beta-\gamma$ spectrum and the systematic error from the peak fitting. For the 765.8-keV transition in ^{95}Nb decay, the second largest uncertainty arises from the determination of the total number of disintegrations, as this decay was only 15% of the total activity at the time of the decay counting.

To determine the β-decay branching ratios for ^{95}Zr, we include the small contribution from conversion electrons (as discussed in Section 1 and presented in Table 2.4). For the decay of ^{95}Nb, the 765.8-keV excited state in ^{95}Mo decays predominantly by γ-ray emission directly to the ground state. This transition is also weakly converted. The 765.8-keV state can also deexcite by a 561.9-keV transition, with an intensity 0.015(3)% that of the higher energy transition. It was not observed in our measurement, but this transition was included in our calculation of the β-branching ratio to the 765.8-keV state.

Table 2.3: The γ-ray branching ratios and contributions to the fractional uncertainty.

E_γ	724.2 keV	756.7 keV	765.8 keV
I_γ	43.57(26)%	54.40(29)%	99.75(102)%
R_{β_γ}	0.0049	0.0041	0.0078
R_β	0.0011	0.0011	0.0057
ϵ_γ	0.0030	0.0030	0.0030
$\epsilon_\beta/\epsilon_{\beta'}$	0.0001	0.0001	0.0001
Total	0.0059	0.0052	0.0102

For the transitions of interest, the resulting β branching ratios, or β transition strengths, I_β, for the transitions of interest obtained from the CARIBU source are presented in Table 2.4. The branching ratios for the 756.7-keV and 765.8-keV transitions agree to well within 1 σ with the current evaluation [10]. The results for the 724.2-keV transition are different by about 2 σ. With three measurements, the probability that one of the comparisons would show a difference of this size is about 20%, and therefore not that unlikely to occur by chance.

Table 2.4: The γ-ray and β branching ratios for ^{95}Zr and ^{95}Nb obtained in this experiment compared with the most recent NNDC evaluation [10]. The conversion coefficients for each transition are also included.

Isotope	E_γ	I_γ(LLNL)	I_γ(NNDC)	α [10]	I_β(LLNL)	I_β(NNDC)
^{95}Zr	724.2 keV	0.4357(26)	0.4427(22)	0.00157(4)	0.4364(26)	0.4434(22)
^{95}Zr	756.7 keV	0.5440(29)	0.5438(22)	0.00142(3)	0.5448(29)	0.5446(22)
^{95}Nb	765.8 keV	0.9975(102)	0.9981(7)	0.0000147(21)	0.9975(101)	0.9981(7)

Chapter 3

Results for ^{147}Nd γ-ray branching ratios

3.1 Source production and data collection

A radioactive sample of ^{147}Nd was produced in the same way as ^{95}Zr, with the radioactive-ion beam at the CARIBU facility [15, 16]. In this case, the mass slits of the isobar separator were set to select only the ions with mass number-to-charge ratio A/Q=73.5, corresponding to doubly-charged A=147 fission products. Once the beam intensity through the aperture was optimized, a 40 μg/cm^2 (200 nm) thick carbon foil floated on an aluminum holder was moved into the beam path for collection of the fission products. The beam was composed of ^{147}Ce ($T_{1/2}$ = 56.4(10) s) and ^{147}Pr ($T_{1/2}$ = 13.4(3) min), that subsequently decayed to the longer-lived isotope ^{147}Nd ($T_{1/2}$ = 10.98(1)d). Just as in the ^{95}Zr sample collection, the average beam intensity was monitored on an hourly timescale by detection of the characteristic γ rays from the decay of short-lived fission products deposited in the foil.

Over a collection time of 64 hours (including the beam-off time), the activities deposited on the foil yielded 1400 Bq of ^{147}Nd. We used the time-history of the collection to gauge not only the number of ^{147}Nd atoms accumulated on the foil but also to calculate the ^{147}Nd-to-^{147}Pm (parent-to-daughter) ratio in the sample over the course of the experiment. Following the end of the sample collection at CARIBU, the foil was shipped to TAMU for high-precision decay counting. The foil was inserted into the center of the 4π gas proportional counter for β-particle detection. The source-detector distance was 152.87(10) mm, as confirmed by measurements with a laser system [29] made subsequent to the experiment.

Coincidence data were collected in cycles for 54.93 s out of every 60 s [33, 32] over a time span of 4.7 days with the KmaxNT system, and a total measurement time of 3.76×10^5 s (6855 cycles). The total measurement time for γ-ray singles, recorded with MAESTRO in parallel with the coincidence system, was nearly 5.4 days (live time of 4.70×10^5 s).

3.2 Coincidence rates ($R_{\beta\gamma}$)

We produced a γ-ray spectrum free of random-coincidence events by first gating on the prompt time-difference peak and then subtracting normalized random coincidences obtained by gating on the flat regions on either side of the prompt peak. The resulting $\beta - \gamma$ coincidence spectrum is shown in Fig. 3.1. To obtain the peak areas, we used the fitting procedure described in Section 2, which is the same one used for the efficiency calibration of the HPGe detector, to determine the number of counts in the peaks by integrating the spectrum above a well-defined background. We were able to determine the number of counts for 12 peaks, with the weakest one having an absolute intensity of only about 0.03%.

The two most intense γ-ray transitions in the decay are presented in Fig. 3.2. The number of counts in the peaks at 91.1 and 531.0 keV were determined to be $1.22(1) \times 10^6$ and $2.046(4) \times 10^5$, respectively. For the 91.1-keV transition, the uncertainty is dominated by difficulties in characterizing the background on the left side of the peak that was caused by the scattering of these low-energy γ rays from the copper housing on the 4π gas counter.

3.3 4π gas counter and HPGe efficiencies

Like in case of ^{95}Zr, we obtained the 4π gas counter efficiencies from the GEANT4 simulation. The β-particle energy spectra for the decays of ^{147}Nd and ^{147}Pm were generated with

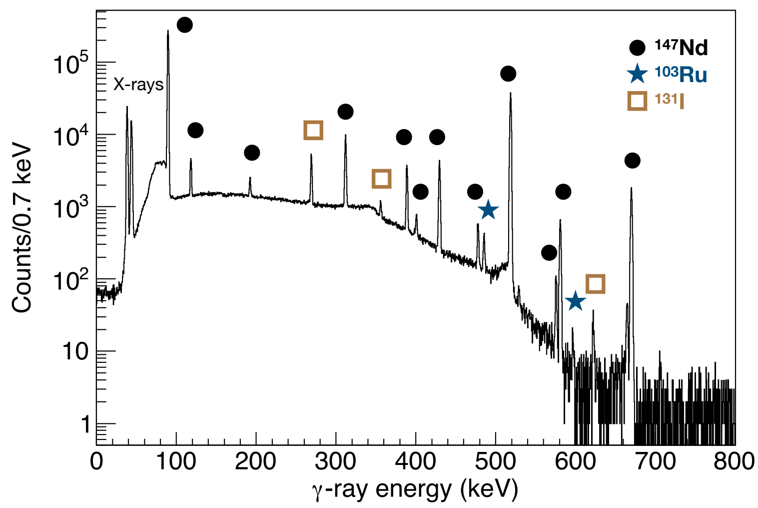

Figure 3.1: The γ-ray spectrum measured in coincidence with β particles. The peaks of interest are labeled by their β-decay parent.

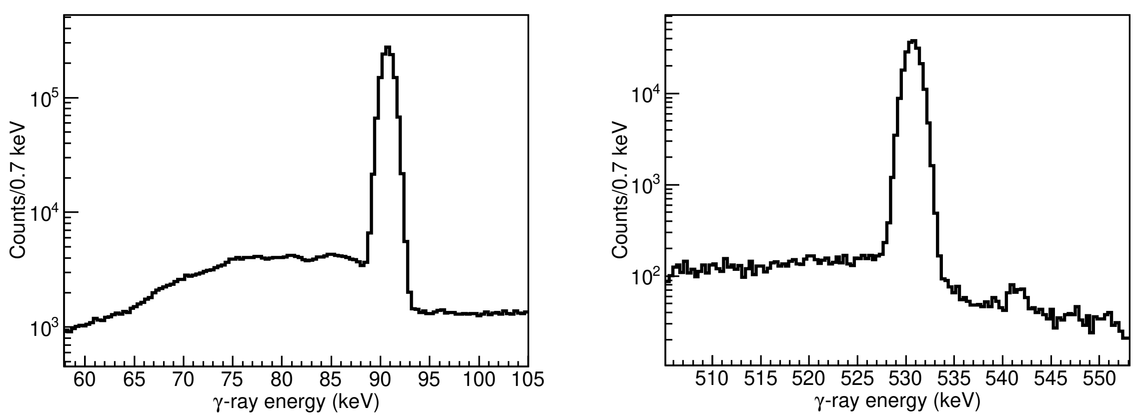

Figure 3.2: Zoomed-in views of the energy regions encompassing the 91.1-keV γ ray (left) and the 531.0-keV γ ray (right) measured in coincidence with β particles.

a Monte Carlo decay code [35] and the resulting spectra are shown in Fig. 3.3. The energy distributions of the β particles emitted from both nuclei are heavily weighted towards low energies with the peaks of the distribution being at nearly zero energy, just as was the case for the ^{95}Zr and ^{95}Nb decays.

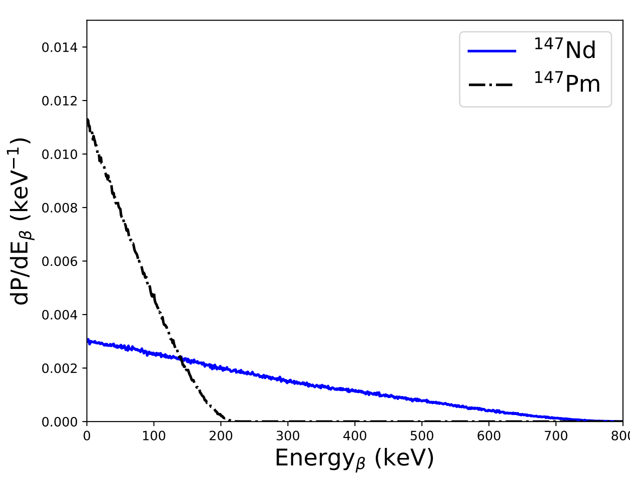

Figure 3.3: Theoretical probability distribution functions for the β-energy spectra from the decays of ^{147}Nd and ^{147}Pm. Both distributions yield a large number of low-energy β particles due to the small Q values and the relatively large Z of the nuclei.

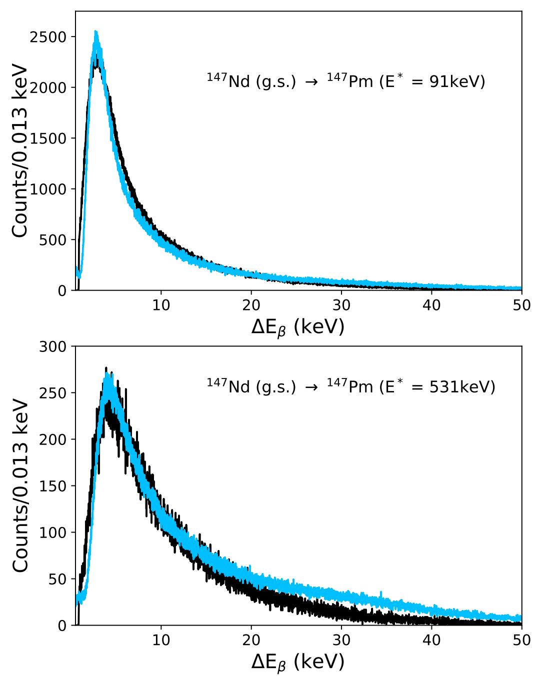

Figure 3.4: Energy deposition in the 4π gas counter detector from the β particles detected in coincidence with the 91.1-keV γ rays and 531.0-keV γ rays from the decay of ^{147}Nd. The measured spectra (black) are compared to the simulation results (blue).

We compared the simulated values with the absolute efficiencies for the transitions, $\epsilon_{\beta'}$, obtained from the data with the ratio of the $R_{\beta\gamma}$ coincident rate to the singles rate R_γ of that particular γ ray. To determine the γ-ray peak areas we used the γ-ray singles spectrum after background subtraction and the same fitting procedure as for the coincidence spectra explained earlier in this section. The coincidence and singles data were collected using two different data acquisition systems and had slightly different measurement times. Therefore, to directly compare the rates, we applied a decay correction to account for a 0.1% difference in average activity expected at the time of the measurement due to the decay of the source.

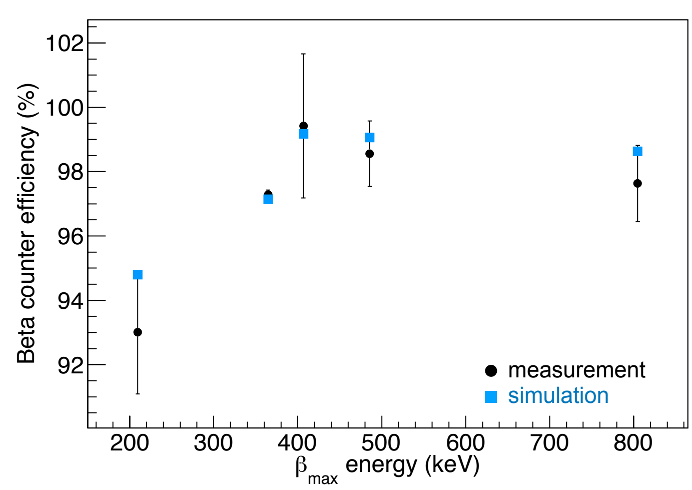

Figure 3.5: Comparison of the measured gas counter efficiencies for the transitions in ^{147}Nd to simulation results with a 0.7-keV threshold.

A comparison of the most intense transitions from the decay of ^{147}Nd with GEANT4 simulation results using the 0.7-keV threshold determined from the analysis of the ^{95}Zr sample is shown in Fig. 3.5. The resulting 4π gas counter efficiencies for detecting the β particles emitted in coincidence with the 91.1, 319.4, 398.2, 531.0 and 685.9-keV γ rays (with corresponding β end point energies of 804.9, 485.7, 406.8, 364.7 and 209.4, respectively) were determined to be 97.6(12)%, 98.6(10)%, 99.4(22)%, 97.3(2)% and 93.0(19)%. The two show excellent agreement, and we used this threshold to determine the simulated total efficiency for detecting ^{147}Nd in the 4π gas counter to be 99.1(2)%. The list of simulated efficiency ratios $\epsilon_\beta/\epsilon_{\beta'}$ for all transitions used in the γ-ray branching ratio determinations, is presented in Table 3.1.

The HPGe detection efficiencies at 152.87(10) mm are reported in Table 3.1. Just like in the case for ^{95}Zr, the efficiencies were about 2.2% smaller than what would have applied at the nominal calibration distance of 151.0 mm, and were assigned slightly higher relative uncertainties (0.3% as compared to 0.2%).

Table 3.1: Detector efficiencies for the γ rays in the decay of ^{147}Nd and the β particle efficiency ratio for the 4π gas counter.

E_γ (keV)	ϵ_γ (%)	$E_{\beta_{max}}$ (keV)	$\varepsilon_\beta/\varepsilon_{\beta'}$
91.1	0.9705(29)	804.9	1.005(2)
120.5	0.9240(29)	364.9	1.000(2)
196.6	0.7496(23)	210.1	1.009(2)
275.7	0.5996(18)	210.1	1.009(2)
319.4	0.5385(16)	485.5	1.001(2)
398.2	0.4565(18)	406.8	1.000(2)
439.9	0.4259(17)	364.9	1.001(2)
489.2	0.3930(15)	406.8	1.017(2)
531.0	0.3699(11)	364.9	1.020(2)
589.4	0.3431(15)	215.6	1.008(2)
594.8	0.3410(15)	210.1	1.009(2)
685.9	0.3082(9)	210.1	1.045(2)

3.4 Determination of R_β

A total of 4.3791×10^8 counts were recorded in the 4π gas counter over the course of the measurement, which resulted in an average detected rate of 1163.12(6) cps above the measured background rate of 0.69(1) cps. The coincidence $\beta-\gamma$ spectrum, shown in Fig. 3.1, revealed the presence of small amount of ^{131}I and ^{103}Ru in the sample, most likely from molecular contaminants in the beam. These disintegrations contribute to the total number of β particles detected in the 4π gas counter, and if not accounted for could lead to lower results of the γ-ray branching ratios. We used the fits of the coincidence spectrum and the absolute intensities of the γ rays in the decay of ^{131}I and ^{103}Ru, at 364.3 keV and 497.2 keV, respectively, to calculate the activity of these isotopes present in the sample at the time of the measurement. The contributions from these two isotopes was estimated to be 0.2% of the total, and the β-particle count rate from ^{147}Nd and ^{147}Pm after subtraction of the background and these isotopic contaminants was determined to be 1160.38(15) cps.

Table 3.2: The contributions to the count rate of the 4π gas counter averaged over the course of the measurement.

Isotope	Decay Rate(cps)
^{147}Nd	1153.63(18)
^{147}Pm	6.76(12)
^{131}I	1.56(13)
^{103}Ru	1.17(5)
Bkg	0.69(1)
Total	1163.81(6)

To obtain the value of R_β for ^{147}Nd and ^{147}Pm, we calculated the fraction each one contributed to the total detected count rate over the course of the measurement based on the time dependence of the implantation at CARIBU and the Bateman equation solutions. Over the time of the coincidence measurement, the fraction of the total activity from the decays of ^{147}Nd and ^{147}Pm were determined to be 0.9939(1) and 0.0061(1), respectively. After accounting for the different β-particle detection efficiency for the two isotopes, the resulting fraction was 0.9942(1) and 0.0058(1). The resulting average decay rates for ^{147}Nd and ^{147}Pm were 1153.63(18) and 6.76(12) cps. The contributions to the 4π gas counter rate are presented in Table 3.2.

3.5 Branching ratios and comparison with previous results

We determined the γ-ray branching ratios, I_γ, for the decay of ^{147}Nd, achieving a relative precision of $0.5 - 1.4\%$ for transitions with absolute intensities greater than 0.3%. The contributions to the uncertainties in the I_γ results for 91.1, 319.4, 398.2, 531.0 and 685.9-keV γ rays are given in Table 3.3. For most transitions, the main component comes from our ability to determine the number of counts in the γ-ray peaks in the $\beta - \gamma$ spectrum. The uncertainty in the peak area is not just a matter of counting statistics – it includes the systematic uncertainty associated with the background subtraction. For example, the counts in the 91-keV peak would be sufficient for a 0.1% statistical precision; however, the background under this peak is difficult to determine because scattering of these γ rays from the 4π gas counter leads to a low-energy shoulder (as can be seen in Fig. 3.2) that has a shape that is difficult to constrain.

Table 3.3: The γ-ray branching ratios and contributions to the fractional uncertainty.

E_γ	91.1 keV	319.4 keV	398.2 keV	531.0 keV	685.9 keV
I_γ	29.017(400)%	1.917(013)%	0.840(009)%	13.019(055)%	0.815(008)%
R_{β_γ}	0.0133	0.0057	0.0096	0.0022	0.0098
R_β	0.0002	0.0002	0.0002	0.0002	0.0002
ϵ_γ	0.0030	0.0030	0.0030	0.0030	0.0030
$\epsilon_\beta/\epsilon_{\beta'}$	0.0020	0.0020	0.0020	0.0020	0.0020
Total	0.0138	0.0067	0.0103	0.0042	0.0104

The complete list of the γ-ray branching ratios we obtained, side-by-side with the values listed in current evaluations [13, 11], are presented in Table 3.4. The ratios of our experimental results to the evaluated values are presented in Figure 3.6.

Table 3.4: The γ-ray branching ratios (in %) compared with the existing evaluations [12, 41] [13, 11]. The values are listed with three digits beyond the decimal place.

γ-ray energy	I_γ(this work)	I_γ(NNDC)	I_γ(DDEP)	I_γ(NDS 1992)
91.1	29.017(400)	28.077(700)	28.400(1800)	27.900(1100)
120.5	0.378(005)	0.376(009)	0.361(014)	0.400(040)
196.6	0.174(006)	0.190(004)	0.180(002)	0.200(020)
275.7	0.776(009)	0.910(019)	0.775(011)	0.800(060)
319.4	1.917(013)	2.127(003)	1.991(019)	1.950(140)
398.2	0.840(009)	0.912(030)	0.855(008)	0.870(070)
439.9	1.189(010)	1.275(030)	1.203(011)	1.200(100)
489.2	0.138(004)	0.155(003)	0.136(011)	0.150(010)
531.0	13.019(053)	13.370(300)	12.700(900)	13.090(890)
589.4	0.034(003)	0.039(003)	0.037(002)	0.046(050)
594.8	0.253(005)	0.283(006)	0.265(004)	0.270(020)
685.9	0.815(008)	0.886(018)	0.834(009)	0.810(060)

The comparison of our results and the NNDC evaluation from 2009 shows significant disagreements that are well beyond the uncertainties for many of the transitions. The I_γ values listed in the NNDC evaluation available online [12] are from the results published in Ref. [14], which were the most precise values with relative uncertainties of about 2%.

However, there are several reasons to be dubious about the results presented in Ref. [14], which lists measured γ-ray energies and intensities with very small uncertainties. As an example, the energy of the most intense γ ray emitted in the decay of ^{147}Nd was measured to be 91.004(2) keV, a value with a 2 eV uncertainty that differs from the results of previous measurements by 100 eV [41]. Similar precision is quoted for several of the other highest-intensity transitions, with energies discrepant often by around 10 σ from previous measurements. While the exact values for the energies have little impact on the determination of the γ-ray intensities, it does seem to indicate that the uncertainties have been greatly underestimated. The γ-ray intensities seem to have a similar problem. They are quoted with uncertainties of about 2%, although most of the intensity results are in disagreement, typically systematically 5–10% higher than the values from previous NNDC evaluation from 1992 which was an evaluated average of the previous measurements. Unfortunately, only a

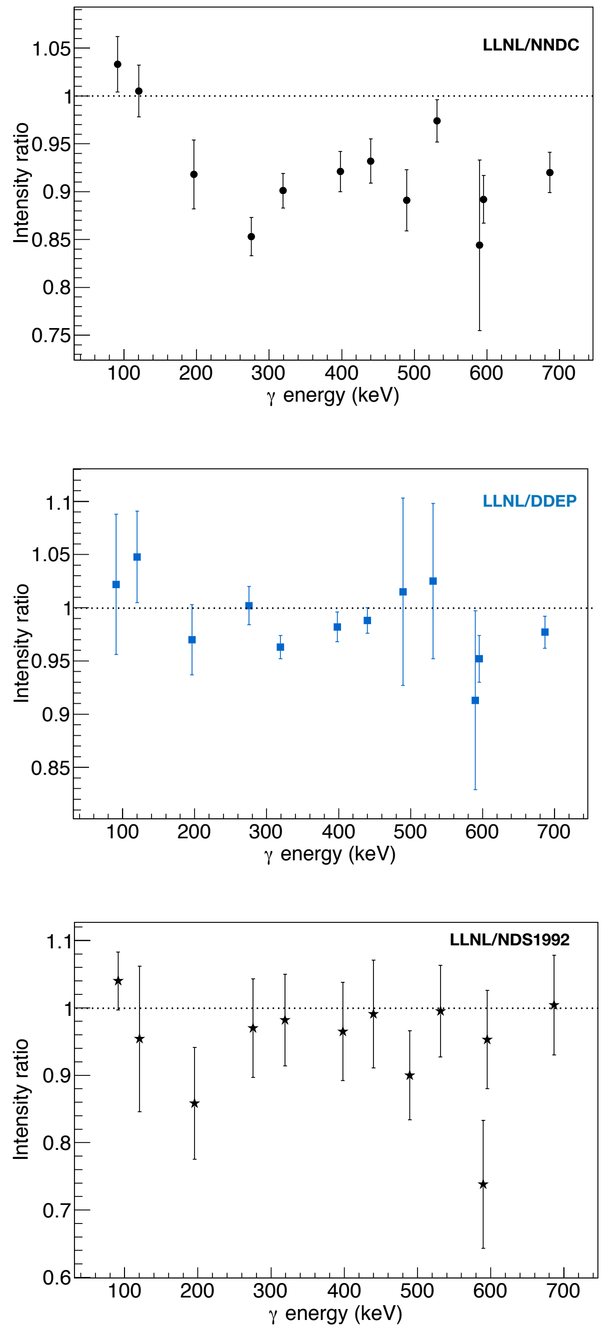

Figure 3.6: The ratio of the γ-rays intensity ratios for the most intense transitions from our work compared with the most recent NNDC evaluation (top) [12], DDEP evaluation [21] (middle), and the NNDC evaluation from 1992 (bottom) [41].

brief description of the experimental setup, detector calibration, data collection, and data analysis is given so it is difficult to determine whether the work was done with sufficient care and scrutiny of systematic effects to justify such high precision. In addition, somewhat strangely, these discrepancies with the previous evaluation in 1992 [41] are never discussed in the paper. Therefore, we believe there is good reason to be doubtful about the precision and reliability of the results presented in Ref. [14].

As can be seen in Figure. 3.6, our results are in reasonable agreement with the DDEP evaluation [21], which incorporates not only on the results from Ref. [14] but also earlier results from Ref. [22], and the earlier NNDC evaluation from 1992 [41], which predated the results from Ref. [14]. For the most intense transitions, we achieved 0.5 – 1.4% precision, which is significantly higher than the uncertainties listed in the evaluations. The reliability of our measurement approach has been demonstrated through detailed studies of the decay of ^{95}Zr, and the systematic uncertainties associated with the detector calibrations have been investigated in detail. Therefore, we recommend using the values obtained here for the γ ray branching ratios from the decay of ^{147}Nd.

Chapter 4

Conclusions

We have demonstrated a new approach to perform precision measurements of γ-ray branching ratios of long-lived fission products and applied it to study the β decays of ^{95}Zr and ^{147}Nd. Radiopure samples of mass-separated short-lived A=95 and A=147 fission products were collected at the CARIBU facility on thin carbon foils. Within a few hours, the short-lived activities decayed to the longer-lived species of interest. The samples were then shipped to TAMU, where we detected the emitted β particles and γ rays in coincidence with a 4π gas counter and a HPGe detector.

Determination of the γ-ray branching ratios depended on a detailed characterization of the performance of the detectors. While the HPGe detector had been efficiency-calibrated through extensive previous work, the response of the 4π gas counter to low-energy β particles was thoroughly investigated here. We developed a GEANT4 model of the detector and compared the simulation results to data. Our comparison of the measured and simulated β-energy spectra from ^{95}Zr and the daughter ^{95}Nb indicated the electronic detection threshold was 0.7(1) keV.

The measurement of the CARIBU-made ^{95}Zr and ^{147}Nd samples led to γ-ray branching ratio results with $0.5 - 1.4\%$ relative precision. We compared the γ-ray branching ratios we measured in the decay of ^{95}Zr to the values in the current evaluations and demonstrated agreement within 1-2σ. We used this approach to determine the γ-ray branching ratios for the decay of ^{147}Nd to high precision. The comparison of our ^{147}Nd results with the current evaluations reveal some discrepancies and lead us to question the accuracy of a previous measurement from 1997. Our results should supersede these previous results.

Bibliography

[1] Robert Vandenbosch and John R. Huizenga. *Nuclear fission.* Academic Press New York, 1973.

[2] M. E. Gooden, C. W. Arnold, J. A. Becker, C. Bhatia, M. Bhike, E. M. Bond, T. A. Bredeweg, B. Fallin, M. M. Fowler, C. R. Howell, J. H. Kelley, Krishichayan, R. Macri, G. Rusev, C. Ryan, S. A. Sheets, M. A. Stoyer, A. P. Tonchev, W. Tornow, D. J. Vieira, and J. B. Wilhelmy. Energy dependence of fission product yields from ^{235}U, ^{238}U and ^{239}Pu for incident neutron energies between 0.5 and 14.8 MeV. *Nuclear Data Sheets*, 131:319 – 356, 2016. Special Issue on Nuclear Reaction Data.

[3] C. Bhatia, B. Fallin, M.E. Gooden, C.R. Howell, J.H. Kelley, W. Tornow, C.W. Arnold, E.M. Bond, T.A. Bredeweg, M.M. Fowler, W.A. Moody, R.S. Rundberg, G. Rusev, D.J. Vieira, J.B. Wilhelmy, J.A. Becker, R. Macri, C. Ryan, S.A. Sheets, M.A. Stoyer, and A.P. Tonchev. Dual-fission chamber and neutron beam characterization for fission product yield measurements using monoenergetic neutrons. *Nuclear Instruments and Methods in Physics Research Section A: Accelerators, Spectrometers, Detectors and Associated Equipment*, 757:7 – 19, 2014.

[4] C. Bhatia, B. F. Fallin, M. E. Gooden, C. R. Howell, J. H. Kelley, W. Tornow, C. W. Arnold, E. Bond, T. A. Bredeweg, M. M. Fowler, W. Moody, R. S. Rundberg, G. Y. Rusev, D. J. Vieira, J. B. Wilhelmy, J. A. Becker, R. Macri, C. Ryan, S. A. Sheets, M. A. Stoyer, and A. P. Tonchev. Exploratory study of fission product yields of neutron-induced fission of ^{235}U,^{238} U, and ^{239}Pu at 8.9 mev. *Phys. Rev. C*, 91:064604, Jun 2015.

[5] M. Bhike, W. Tornow, M. Krishichayan, and A. P. Tonchev. Exploratory study of fission product yield determination from photofission of ^{239}Pu at 11 MeV with monoenergetic photons. *Phys. Rev. C*, 95:024608, Feb 2017.

[6] Krishichayan, Megha Bhike, S.W. Finch, C.R. Howell, A.P. Tonchev, and W. Tornow. Photofission cross-section ratio measurement of 235u/238u using monoenergetic photons in the energy range of 9.0–16.6mev. *Nuclear Instruments and Methods in Physics Research Section A: Accelerators, Spectrometers, Detectors and Associated Equipment*, 854:40 – 44, 2017.

[7] A. P. Tonchev. *6th Intern. Conf. on Fiss. and Prop. of Neutron-Rich Nuclei*, page 381, 2017.

[8] M. A. Stoyer, A. P. Tonchev, J.A. Silano, M.E. Gooden, J.B. Wilhelmy, W. Tornow, C. R. Howell, F. Krishichayan, and S. Finch. Fission product yield measurements from neutron-induced fission of ^{235,238}U and ^{239}Pu. *EPJ Web Conf.*, 232:03006, 2020.

[9] H. D. Selby, M. R. Mac Innes, D. W. Barr, A. L. Keksis, R. A. Meade, C. J. Burns, M. B. Chadwick, and T. C. Wallstrom. Fission Product Data Measured at Los Alamos for Fission Spectrum and Thermal Neutrons on ^{239}Pu, ^{235}U, ^{238}U. *Nuclear Data Sheets*, 111(12):2891 – 2922, 2010. Nuclear Reaction Data.

[10] S. K. Basu, G. Mukherjee, and A. A. Sonzogni. Nuclear data sheets for A = 95. *Nuclear Data Sheets*, 111(10):2555 – 2737, 2010.

[11] Decay Data Evaluation Project http://www.nucleide.org/DDEP_WG/DDEPdata.htm, 2019.

[12] N. Nica. Nuclear data sheets for A = 147. *Nuclear Data Sheets*, 110(4):749 – 997, 2009.

[13] NNDC. National Nuclear Data Center https://www.nndc.bnl.gov, 2019.

[14] M. Sainath, K. Venkataramaniah, and P. C. Sood. Level structures in ^{147}Pm from ^{147}Nd decay. *Phys. Rev. C*, 56:2468–2473, Nov 1997.

[15] G. Savard, S. Baker, C. Davids, A. F. Levand, E. F. Moore, R. C. Pardo, R. Vondrasek, B. J. Zabransky, and G. Zinkann. Radioactive beams from gas catchers: The CARIBU facility. *Nuclear Instruments and Methods in Physics Research Section B: Beam Interactions with Materials and Atoms*, 266(19):4086 – 4091, 2008.

[16] G. Savard, A. F. Levand, and B. J. Zabransky. The CARIBU gas catcher. *Nuclear Instruments and Methods in Physics Research Section B: Beam Interactions with Materials and Atoms*, 376:246 – 250, 2016.

[17] J. C. Hardy, V. E. Iacob, M. Sanchez-Vega, R.T. Effinger, P. Lipnik, V. E. Mayes, D. K. Willis, and R. G. Helmer. Precise efficiency calibration of an HPGe detector: source measurements and Monte Carlo calculations with sub-percent precision. *Applied Radiation and Isotopes*, 56(1):65 – 69, 2002. Proceedings of the Conference on Radionuclide Metrology and its A pplications, ICRM'01.

[18] R. G. Helmer, J. C. Hardy, V. E. Iacob, M. Sanchez-Vega, R. G. Neilson, and J. Nelson. The use of monte carlo calculations in the determination of a ge detector efficiency curve. *Nuclear Instruments and Methods in Physics Research Section A: Accelerators, Spectrometers, Detectors and Associated Equipment*, 511(3):360 – 381, 2003.

[19] R. G. Helmer, N. Nica, J. C. Hardy, and V. E. Iacob. Precise efficiency calibration of an HPGe detector up to $3.5mev$, with measurements and Monte Carlo calculations. *Applied Radiation and Isotopes*, 60(2):173 – 177, 2004.

[20] T. Kibédi, T.W. Burrows, M.B. Trzhaskovskaya, P.M. Davidson, and C.W. Nestor. Evaluation of theoretical conversion coefficients using BrIcc. *Nuclear Instruments and Methods in Physics Research Section A: Accelerators, Spectrometers, Detectors and Associated Equipment*, 589(2):202 – 229, 2008.

[21] C. Dulieu M. M. Be, V. Chiste. Table of radionuclides. *DDEP 7 of Monographie BIPM-5. Pavillon de Breteuil*, 7, 2013.

[22] N.A. Voinova, A.A. Rodionov, Y.V. Sergeenkov, P.A. Sushkov, and M.A. Elizbarashvili. The decay of ^{147}nd. *Izv. Akad. Nauk SSSR*, 43, 1979.

[23] C. N. Davids and D. Peterson. A compact high-resolution isobar separator for the CARIBU project. *Nuclear Instruments and Methods in Physics Research Section B: Beam Interactions with Materials and Atoms*, 266(19):4449 – 4453, 2008. Proceedings of the XVth International Conference on Electromagnetic Isotope Separators and Techniques Related to their Applications.

[24] V. T. Koslowsky, E. Hagberg, J. C. Hardy, R. E. Azuma, E. T. H. Clifford, H. C. Evans, H. Schmeing, U. J. Schrewe, and K. S. Sharma. The half-lives of ^{26m}Al, ^{34}Cl, ^{38m}K: Precision measurements with isotope-separated samples. *Nuclear Physics A*, 405(1):29 – 39, 1983.

[25] V. T. Koslowsky, E. Hagberg, J. C. Hardy, G. Savard, H. Schmeing, K. S. Sharma, and X. J. Sun. The half-lives of ^{42}Sc, ^{46}V, ^{50}Mn, and ^{54}Co. *Nuclear Instruments and Methods in Physics Research Section A: Accelerators, Spectrometers, Detectors and Associated Equipment*, 401(2):289 – 298, 1997.

[26] B. Champine. *Experiments to Improve Nuclear Data for High Energy Density Environments*. PhD thesis, UC Berkeley, 2016.

[27] V. E. Iacob, J. C. Hardy, L. Chen, V. Horvat, M. Bencomo, N. Nica, H. I. Park, B. T. Roeder, and A. Saastamoinen. Precise half-life measurement of the superallowed emitter ^{30}S. *Phys. Rev. C*, 97:035501, Mar 2018.

[28] J. A. Halbleib, R. P. Kemsek, T. A. Mehlhorn, et al. Report sand 91-16734. *Sandia National Labs*, 1992.

[29] AcuityLaser http://www.acuitylaser.com, 2019.

[30] Sparrowcorp http://www.sparrowcorp.com, 2019.

[31] H. I. Park, J. C. Hardy, V. E. Iacob, M. Bencomo, L. Chen, V. Horvat, N. Nica, B. T. Roeder, E. Simmons, R. E. Tribble, and I. S. Towner. β decay of ^{38}Ca: Sensitive test of isospin symmetry-breaking corrections from mirror superallowed $0^+ \to 0^+$ transitions. *Phys. Rev. Lett.*, 112:102502, Mar 2014.

[32] H. I. Park, J. C. Hardy, V. E. Iacob, M. Bencomo, L. Chen, V. Horvat, N. Nica, B. T. Roeder, E. McCleskey, R. E. Tribble, and I. S. Towner. Precise measurement of branching ratios in the β decay of ^{38}Ca. *Phys. Rev. C*, 92:015502, Jul 2015.

[33] V. E. Iacob, J. C. Hardy, C. A. Gagliardi, J. Goodwin, N. Nica, H. I. Park, G. Tabacaru, L. Trache, R. E. Tribble, Y. Zhai, and I. S. Towner. Branching ratios for the β decay of ^{21}Na. *Phys. Rev. C*, 74:015501, Jul 2006.

[34] D.C Radford. ESCL8R and LEVIT8R: Software for interactive graphical analysis of hpge coincidence data sets. *Nuclear Instruments and Methods in Physics Research Section A: Accelerators, Spectrometers, Detectors and Associated Equipment*, 361(1):297 – 305, 1995.

[35] N. D. Scielzo, S. J. Freedman, B. K. Fujikawa, and P. A. Vetter. Measurement of the $\beta - \nu$ correlation using magneto-optically trapped ^{21}Na. *Phys. Rev. Lett.*, 93:102501, Aug 2004.

[36] N. F. Mott and H. S. W. Massey. *The Theory of Atomic Collisions*. Clarendon Press, 1933.

[37] H. Behrens and J. Jänecke. *Numerical Tables for Beta-Decay and Electron Capture*. Springer-Verlag, 1969.

[38] SRIM. The Stopping and Range of Ions in Matter http://www.srim.org, 2019.

[39] S. Agostinelli et al. Geant4—a simulation toolkit. *Nuclear Instruments and Methods in Physics Research Section A: Accelerators, Spectrometers, Detectors and Associated Equipmexnt*, 506(3):250 – 303, 2003.

[40] S.M. Seltzer, J.M. Fernandez-Varea, P. Andreo, P.M. Bergstrom, D.T. Burns, I. Krajcar Bronic, C.K. Ross, and F. Salvat. Report 90: key data for ionizing-radiation dosimetry: measurement standards and application.

[41] E. Der Mateosian and L. K. Peker. Nuclear data sheets for A = 147. *Nuclear Data Sheets*, 66(705):705 – 838, 1992.